AGU PUBLICATIONS

JGR

Journal of Geophysical Research: Solid Earth

RESEARCH ARTICLE
10.1002/2017JB014278

**Key Points:**
- Subaerial topographic growth on the Lhasa terrane of the Tibetan Plateau initiated at early Albian time (ca. 111 Ma)
- Cretaceous marine regression on the Lhasa terrane was diachronous, progressive from east to west
- Initial topographic growth on the Lhasa terrane was tectonically controlled by the Lhasa-Qiangtang collision

**Supporting Information:**
- Supporting Information S1

**Correspondence to:**
J.-G. Wang,
wangjiangang@mail.iggcas.ac.cn

**Citation:**
Wang, J.-G., X. Hu, E. Garzanti, W.-Q. Ji, Z.-C. Liu, X.-C. Liu, and F.-Y. Wu (2017), Early cretaceous topographic growth of the Lhasaplano, Tibetan plateau: Constraints from the Damxung conglomerate, *J. Geophys. Res. Solid Earth*, *122*, doi:10.1002/2017JB014278.

Received 4 APR 2017
Accepted 28 JUN 2017
Accepted article online 4 JUL 2017



# Early cretaceous topographic growth of the Lhasaplano, Tibetan plateau: Constraints from the Damxung conglomerate

**Jian-Gang Wang[1], Xiumian Hu[2], Eduardo Garzanti[3], Wei-Qiang Ji[1], Zhi-Chao Liu[4], Xiao-Chi Liu[1], and Fu-Yuan Wu[1]**

[1]State Key Laboratory of Lithospheric Evolution, Institute of Geology and Geophysics, Chinese Academy of Sciences, Beijing, China, [2]State Key Laboratory of Mineral Deposits Research, School of Earth Sciences and Engineering, Nanjing University, Nanjing, China, [3]Departmentof Earth and Environmental Sciences, Università di Milano-Bicocca, Milan, Italy, [4]School of Earth Science and Geological Engineering, Sun Yat-Sen University, Guangzhou, China

**Abstract** Constraining the timing of early topographic growth on the Tibetan plateau is critical for any models of India-Asia collision, Himalayan orogeny and subsequent plateau development in the Cenozoic. Stratigraphic, sedimentological and provenance analysis of the Lower Cretaceous red-beds of the Damxung Conglomerate provide new key information to reconstruct the paleogeography and the tectonic evolution of the Lhasa terrane at the time. The over 700-m-thick Damxung Conglomerate documents distal alluvial fan to braidplain sedimentation passing upward to proximal alluvial fan sedimentation. Deposition began near sea level, as documented by limestone beds occurring at the base of the unit. Zircon U–Pb dating of interbedded tuff layers constrain deposition age at ca. 111 Ma. Abundance of volcanic clasts, Cretaceous U–Pb ages and Hf isotopes of detrital zircons yielding mainly negative $\varepsilon_{Hf}(t)$ values together with paleocurrent data indicate an active volcanic source located in the North Lhasa subterrane. Pre-Mesozoic-aged zircon, recycled quartz and (meta) sedimentary rock fragments increase up-section, indicating progressive erosional exhumation of the Paleozoic sedimentary/metasedimentary basement. The Damxung Conglomerate thus records a significant uplift and unroofing stage in the source region, implying initial topographic growth on the Lhasa terrane at early Albian time. Early Cretaceous topographic growth on the Lhasa terrane is supported by the stratigraphic record in the Linzhou basin, the Xigaze forearc basin and the southern Nima basin. In contrast, marine strata in the central-western Lhasa terrane lasted until the early Cenomanian (ca. 96 Ma), indicating diachronous marine regression on the Lhasa terrane from east to west.

## 1. Introduction

The formation of the Tibetan Plateau, which today has an average elevation over 5000 meters, has exerted substantial control over the Asian climate, monsoon intensity, and ocean chemistry [*Raymo and Ruddiman*, 1992; *Richter et al.*, 1992; *An et al.*, 2001]. It is widely believed that the Tibetan Plateau is essentially a late Cenozoic feature produced by the India-Asian collision [e.g., *Molnar*, 2005], although diverse evidences have indicated that the Tibetan Plateau had undergone significant crustal shortening, uplift and exhumation prior to Paleocene India-Asia collision [e.g., *Murphy et al.*, 1997; *P. Kapp et al.*, 2005; *Kapp et al.*, 2007a; *Leier et al.*, 2007a; *Sun et al.*, 2015]. Early topographic growth on the plateau was generally ascribed to subduction and collision along major suture zones in Tibet [e.g., *Murphy et al.*, 1997; *Kapp et al.*, 2007b], but uplift history and tectonic control during such early stages have remained poorly understood.

The Tibetan Plateau consists of several east–west elongated tectonic domains (herein called generically "terranes" and "subterranes") accreted progressively to the southern margin of Eurasia during the Phanerozoic (Figure 1a) [*Allègre et al.*, 1984]. The Lhasa terrane, a fundamental constituent of the Tibetan Plateau, was accreted to the southern Asian margin well before the India-Asia collision [*Yin and Harrison*, 2000]. Constraints on the geomorphologic evolution of the Lhasa terrane are critical to assess the timing of early topographic growth in Tibet, and to provide initial conditions for models of Cenozoic orogeny and plateau development. Tectonic and sedimentary studies have documented substantial crustal shortening and erosion of the Lhasa terrane in the Cretaceous [*Murphy et al.*, 1997; *P. Kapp et al.*, 2005; *Kapp et al.*, 2007a]. During the Early-early Late Cretaceous, widespread limestone deposition in shallow marine was replaced by continental red beds [*Zhang et al.*, 2004, 2012; *Leier et al.*, 2007a; *Zhang et al.*, 2011; *Sun et al.*, 2015;

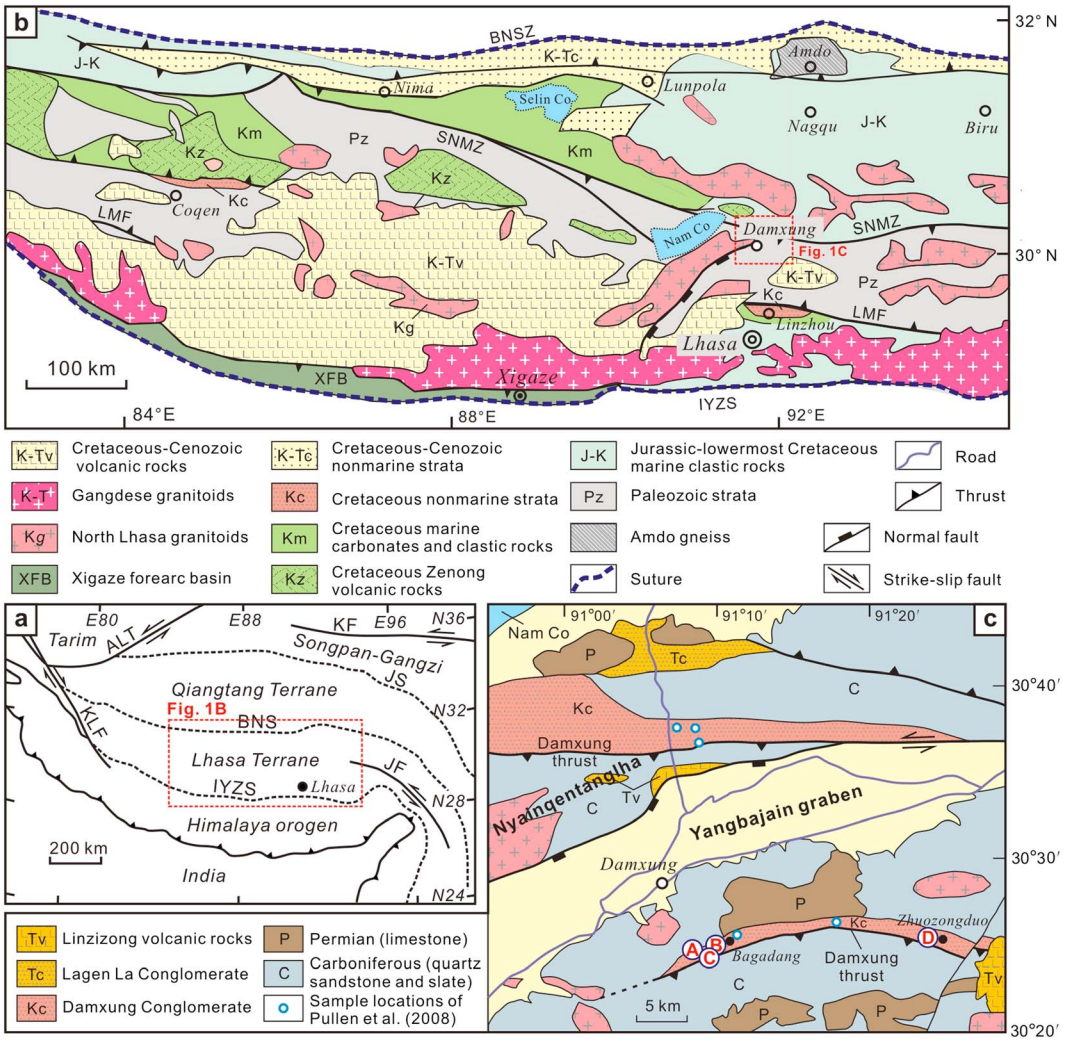


**Figure 1.** (a) Simplified tectonic map of the Himalaya-Tibetan Plateau showing major terranes, suture zones and faults. ALT, Altyn Tagh fault; BNS, Bangong–Nujiang suture; IYZS, Indus–Yarlung-Zangbo suture; JF, Jiali fault; JS, Jinshajiang suture; KF, Kunlun fault; KLF, Karakoram fault. (b) Simplified geological map of the Lhasa terrane after *P. Kapp et al.* [2005]. LMF, Luobadui-Milashan fault; SNMZ, Shiquan River-Nam Tso melange zone. (c) Geological map of the Damxung area (after the Chinese 1:250 000 Damxung geological map), indicating sites of measured sections in this study and zircon samples of *Pullen et al.* [2008].

*Boudagher-Fadel et al.*, 2017], which were strongly folded and eventually overlain unconformably by the midly deformed Linzizong Group volcanic succession in the early Paleogene [*Murphy et al.*, 1997; *He et al.*, 2007]. An estimate of crustal shortening has suggested that the Lhasa terrane might have been raised from nearly sea level to as much as 3–4 km prior to Paleogene India-Asian collision [*Murphy et al.*, 1997]. However, it has not been established yet whether Cretaceous shortening and tectonic uplifting of the Lhasa terrane was controlled by subduction of Neotethyan oceanic lithosphere along its southern boundary [*Leier et al.*, 2007a; *Kapp et al.*, 2007b] or by collision with the Qiangtang terrane along its northern boundary [*Murphy et al.*, 1997; *P. Kapp et a.*, 2005; *Sun et al.*, 2015].

In order to determine the timing of initial topographic growth on the Lhasa terrane and to test tectonic models for its evolution, we have carried out an integrated stratigraphic, sedimentological, geochronological and provenance study on Cretaceous red-beds exposed in the Damxung area of the eastern Lhasa terrane (Figures 1b and 1c). By LA–ICP–MS dating of zircon crystals from tuffs and detrital grains from sandstones, we can access the precise age of initial deposition of alluvial fan conglomerates, which document uplift and erosion of the northern Lhasa subterrane that is interpreted to have resulted from collision with the Qiangtang terrane in the north.

## 2. Geological Setting

### 2.1. Regional Geology

The Lhasa terrane was the last continental block accreted to the southern margin of Asia before collision with India [*Yin and Harrison*, 2000]. It is welded to the Qiangtang terrane by the Bangong-Nujiang suture in the north and to the Tethys Himalaya, representing the northern passive margin of India [*Sciunnach and Garzanti*, 2012], by the Yarlung-Zangbo suture in the south (Figure 1a). Collision between the Qiangtang and Lhasa terranes occurred roughly during the Late Jurassic to the Early Cretaceous time [*Marcoux et al.*, 1987; *Dewey et al.*, 1988; *P. Kapp et al.*, 2005], while the India-Lhasa collision was initiated in the Middle Paleocene [*Hu et al.*, 2015].

The Lhasa terrane is traditionally subdivided into the South Lhasa and North Lhasa subterranes by the eclogite- and blueschist-bearing metamorphic belt along the Luobadui-Milashan fault [*Yang et al.*, 2009; *Liu et al.*, 2010] (Figure 1b). The South Lhasa subterrane comprises upper Mesozoic–lower Cenozoic Gangdese arc batholiths and related volcanic rocks, which resulted from northward subduction of Neotethyan oceanic lithosphere [e.g., *Wen et al.*, 2008; *Lee et al.*, 2009]. Magmatic rocks in the Gangdese arc are characterized by extremely depleted Hf isotopes, indicating a juvenile source [e.g., *Ji et al.*, 2009; *Zhu et al.*, 2011a]. The sedimentary cover of the South Lhasa subterrane is limited and mainly Jurassic–Cretaceous in age [e.g., *Leier et al.*, 2007a, 2007b].

The North Lhasa subterrane [including the central and north Lhasa subterranes of *Zhu et al.* [2011a]] also documents long-term Mesozoic–Cenozoic magmatism, associated with either southward subduction of Bangong-Nujiang oceanic lithosphere in the north [e.g., *Zhu et al.,* 2011a] or northward subduction of the Neotethyan oceanic lithosphere in the south [e.g., *P. Kapp et al.*, 2005]. Geochronological studies have revealed a magmatic flare up at 113 ± 5 Ma [*Hou et al.*, 2015]. Igneous rocks in the North Lhasa subterrane commonly yield enriched Hf isotopes indicating re-melting of older crust [e.g., *Chu et al.*, 2006; *Chiu et al.*, 2009; *Zhu et al.*, 2011a]. A few bodies dated around ~113 Ma have instead depleted Hf isotopes, indicating significant mantle contribution [*Chen et al.*, 2014]. Pre-Cretaceous sedimentary covers are widely exposed and include Carboniferous quartz-sandstones, Permian limestones and Jurassic siliciclastic rocks [*Yin et al.*, 1988; *Pan et al.*, 2004].

Cretaceous strata are widespread across the Lhasa terrane, and were deposited into two domains separated by the Gangdese magmatic arc (Figure 1b). To the south of the Gangdese arc, the Xigaze forearc basin was filled mainly by a shallowing-upward lowermost Albian to Lower Eocene clastic megasequence mostly fed from the Gangdese magmatic arc, including deep-sea turbidites in the lower part and fluvio-deltaic sediments at the top [*Wang et al.*, 2012; *An et al.*, 2014; *Orme et al.*, 2015; *Orme and Laskowski*, 2016; *Wang et al.*, 2017]. North of the Gangdese arc, sedimentary basins (e.g., Coqen, Nyima, Selin Co and Linzhou basins) were filled by shallow-marine volcaniclastic sandstones, limestones and continental clastic sediments [*DeCelles et al.*, 2007; *Leier et al.*, 2007a; *Zhang et al.*, 2011; *Sun et al.*, 2015].

### 2.2. Geology of the Damxung Area

The study area is located near Damxung, on the North Lhasa subterrane (Figure 1c). Widespread Paleozoic strata, including Carboniferous quartzites and slates, and Permian limestones, were intruded by Mesozoic–Cenozoic granitoids and overlain with angular unconformity by locally preserved Lower Cenozoic Linzizong Group volcanic rocks. The Paleozoic strata were downthrown by the Yangbajain graben, the most important structure in this area flanked on its northwestern side by the Nyainqentanglha Range [*Harrison et al.*, 1995; *J. L. Kapp et al.*, 2005].

The Cretaceous red beds that we have studied in detail crop out on the eastern side of the Yangbajain Graben, ~10 km southeast of Damxung village (Figure 1c), where they are better exposed and far more continuous than on the northwestern flank of the Nyainqentanglha Range. The strata were designated as Shexing Formation in the 1:250,000 Chinese regional geological map or as the Lhunzhub member of the Takena Formation in international literature [e.g., *Leier et al.*, 2007a], based on correlation with the Cretaceous red beds of the Linzhou basin. However, our studies revealed that red beds exposed in the Damxung area show quite different sedimentary facies and provenance from continental red beds of the Linzhou basin (as discussed further below). We propose that these beds are designated a new stratigraphic unit - Damxung Conglomerate. This coarse-grained clastic unit stratigraphically unconformably

overlies Lower Cretaceous volcanic rocks or Paleozoic metasedimentary basement, and is tectonically overlain by the north-verging Damxung thrust with Paleozoic strata in the hanging wall [*Pullen et al.*, 2008].

## 3. Methods

Stratigraphy and sedimentary environments of the Damxung Conglomerate were studied by detailed logging and sedimentological observations on four measured sections with a total thickness of over 700 meters (Figure 2). The adopted lithofacies scheme is mainly after *Miall* [1978] and *DeCelles et al.* [1991]. Stratigraphic correlation among different sections was based on field relationships, petrography and sedimentary facies. Paleocurrent data were collected by measuring dips of trough cross-lamination following the approach described by *DeCelles et al.* [1983]. Depositional age was determined by zircon U–Pb dating of tuffs interbedded in the lower part of the succession.

Petrographic data integrated with U–Pb ages and Hf isotopes of detrital zircons were used to trace the sedimentary source of the Damxung Conglomerate. Gravel composition was dertermined by counting ~100 clasts at each site, using a 10 × 10 cm or 5 × 5 cm grid depending on clast size. Detrital modes of sandstones were determined by counting ~400 points per thin sections following the Gazzi-Dickinson method [*Ingersoll et al.*, 1984].

Zircon grains were handpicked randomly, mounted in epoxy resin and then polished to produce a smooth, flat surface. Cathodoluminescence images were obtained to reveal their internal structure. U–Pb dating and Hf isotope analyses of zircons were conducted at the State Key Laboratory of Lithosphere Evolution, Institute of Geology of Geophysics, Chinese Academy of Sciences. Analytical results are given in Appendix tables.

Detrital zircons were dated by Laser Ablation–Inductively Coupled Plasma–Mass Spectrometry (LA–ICP–MS). Details of instrumental conditions and data acquisition are as in *Xie et al.* [2008]. A spot diameter of 44 μm was used during the analysis. The raw count rates for $^{206}Pb$, $^{207}Pb$, $^{208}Pb$, $^{232}Th$ and $^{238}U$ were collected for age determination. $^{207}Pb/^{206}Pb$ and $^{206}Pb/^{238}U$ ratios were calculated using the GLITTER program (GEMOC, Macquarie University) [*Griffin et al.*, 2008]. Common Pb corrections were performed using the method described in *Andersen* [2002]. Age calculations and plotting of concordia diagrams were performed using Isoplot 3.75 [*Ludwig*, 2012]. The $^{206}Pb/^{238}U$ and $^{207}Pb/^{206}Pb$ ages were used for grains less than and greater than 1000 Ma, respectively. Ages with >10% discordance were discarded.

Hf isotope measurements were performed using a Neptune Multi-Collector ICP–MS equipped with the Geolas 193 laser-ablation system. Details on instrumental conditions and data acquisition are as in *Wu et al.* [2006]. Hf isotope analyses were performed with a spot diameter of 60 μm, overlapping onto the spot used for age-dating. During analysis, average $^{176}Hf/^{177}Hf$ ratios of standard zircons GJ-1 and Mud Tank of 0.282019 ± 25 (2SD) and 0.282514 ± 25 (2SD) were obtained, consistently with reported values [*Morel et al.*, 2008; *Woodhead and Hergt*, 2005]. To calculate the $\varepsilon_{Hf}(t)$ value and the 'crustal' model age ($T_{DM}^{C}$), we adopted a depleted mantle model with $^{176}Hf/^{177}Hf = 0.28325$ and $^{176}Lu/^{177}Hf = 0.0384$ [*Griffin et al.*, 2000], and chondrite values of $^{176}Hf/^{177}Hf = 0.282772$ and $^{176}Lu/^{177}Hf = 0.0332$ [*BlichertToft and Albarède*, 1997]. We assumed an average continental crustal $^{176}Lu/^{177}Hf$ ratio of 0.015 for the protolith of the host magma [*Griffin et al.*, 2002] and used a decay constant of $^{176}Lu$–$^{176}Hf$ of $1.867 \times 10^{-11}$ $yr^{-1}$ [*Söderlund et al.*, 2004].

## 4. Sedimentology of the Damxung Conglomerate

The Damxung Conglomerate is a coarse-grained terrigenous suite including mainly red conglomerates, sandstones, mudrocks with minor intercalated tuffs and limestones (Figure 2). Ten clastic lithofacies were identified in the four measured sections (Table 1), where a lower member of stream-dominated, braidplain to distal alluvial fan facies is overlain by an upper member of proximal alluvial fan facies dominated by debris flow deposits.

### 4.1. The Lower Member

#### 4.1.1. Description

The facies association characterizing section A and the lower part of section B (Figure 2) comprises red mudrocks and reddish to grayish sandstones interbedded with pebble conglomerates (Figures 3a, 3b and 3c). Beds of sandstones are laterally continuous for several to over one hundred meters, and commonly display erosional bases (Figure 3a). Bed thickness increases up-section, from several tens of centimeters to

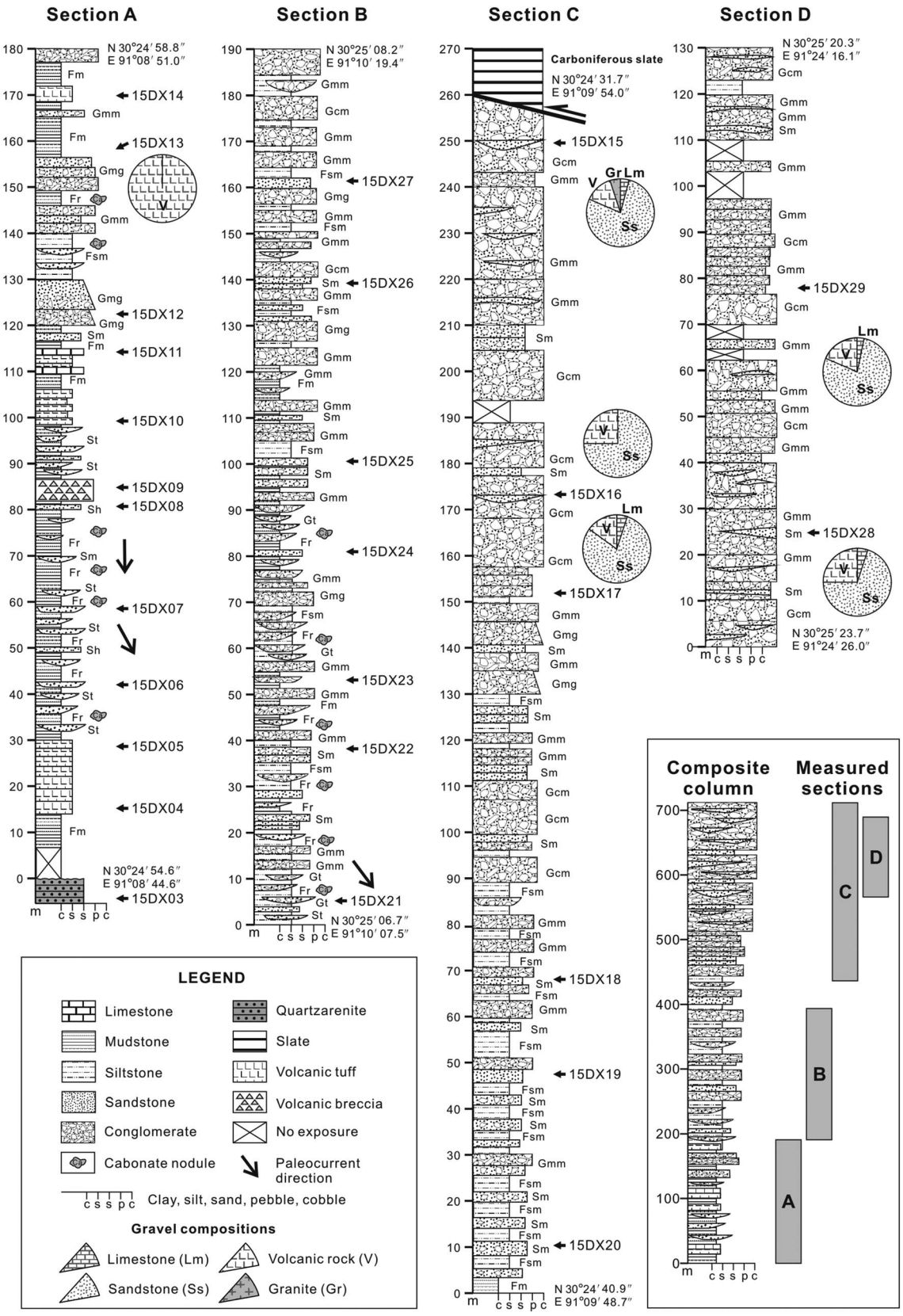


**Figure 2.** Stratigraphic logs of the four measured sections in the Damxung Conglomerate, with lithofacies, sample locations and paleocurrent directions. Pie charts show the composition of conglomerate clasts. A composite stratigraphic column is shown in the lower-right panel.

**Table 1.** Lithofacies From the Damxung Conglomerate and their General Sedimentological Interpretation

| Facies Code | Description | Interpretation |
|---|---|---|
| Gcm | Massive, clastic supported, pebble to cobble conglomerate; subround to angular gravel, poorly to moderately sorted, poorly organized; beds are several tens of centimeters to several meters thick, extends laterally for several to tens of meters | Clast-rich debris flow deposits or channel deposits |
| Gmm | Massive, matrix supported, pebble to cobble conglomerate; subangular to angular gravel, unsorted, disorganized; beds are several tens of centimeters to over one meter thick, extends laterally for tens of meters | Plastic debris flow deposits |
| Gmg | Matrix supported, pebble conglomerate with poorly developed normal grading; subangular to angular gravel, poorly sorted; beds are several tens of centimeters to over one meter thick, extends laterally for tens of meters | Pseudoplastic debris flow deposits |
| Gt | Clastic supported, pebble conglomerate with sandy matrix, poorly developed trough cross-stratification; angular to subround gravel, poorly to moderately sorted; beds are several tens of centimeters thick, extends laterally for tens of meters | Migration of gravelly 3-D dunes under traction flows in braided or fluvial channels |
| Sm | Massive coarse-grained sandstone, generally pebbly, can have poor normal grading; beds are several tens of centimeters thick, extends laterally for tens of meters | Sand-rich debris flow deposits |
| St | Medium- to coarse-grained sandstone, lense shape, trough cross-stratified; beds are several tens of centimeters thick, laterral continuous for only several to over ten meters | Migration of 3-D ripples (dunes) under moderately powerful unidirectional flows in shallow channels |
| Sh | Fine- to medium-grained sandstone with parallel lamination; 10 to 30 cm bed thick | Upper plane bed conditions under strong or very shallow unidirectional flows |
| Fsm | Red massive siltstone beds, can contain a few gravels and rare carbonate nodules; beds varies from 0.1 to 2 meters thick | Waning flows, overbank floods deposits; paleosols |
| Fr | Massive to laminated, mottled mudstone, unsually red; occationally bioturbated, carbonate nodules common | Waning flows, overbank floods deposits; calcic paleosols |
| Fm | Red massive mudtone | Waning flows, overbank floods deposits |

~4 meters. Poorly developed trough cross-lamination is observed occasionally (facies St) (Figure 3b). Clasts of sandstones are generally coarse grained, and commonly associated with pebble to cobble clasts. The conglomerates generally occur at the base of sandstone beds. They are clastic or sandy-matrix supported and include poorly sorted, fine- to medium-grained, angular to subangular pebbles (Gmm). Massive red mudrocks contain carbonate nodules and common burrows (Fr and Fm).

Thin-bedded to massive, white to reddish tuffs or volcanic breccia layers are frequently intercalated in the lowermost part of the succession (Figure 2). Tuffs are commonly felsitic, with quartz and sanidine phenocrysts (Figure 4a). Two micritic limestone beds (each ~40-cm thick) in the lower part of section A (Figure 2) contain recrystallized bioclasts (Figure 4b).

#### 4.1.2. Interpretation

The lithofacies association, with pebbly, trough cross-laminated sandstones and lack of muddy matrix in coarse-grained sediments indicating traction effects, suggests deposition in a stream-dominated environment which probably occurred in the distal alluvial fans or in a braidplain [*Ridgway and DeCelles*, 1993; *DeCelles et al.*, 1991]. Lithofacies St, Sm, Gt and Gmm are interpreted as braided-river deposits, whereas lithofacies Fr, Fm, and Fsm represent sediments deposited by waning debris flows or overbank floods (Table 1). Biomicrites at the base of the succession testify to a subaqueous environment. However, we cannot be certain it was a lake or a shallow marine since the bio-clasts were all recrystallized. We tend to interpret it as a shallow marine environment because the fossils are diverse in shape, whereas fossils in lacustrine carbonates commonly show very low degree of differentiation [*Gierlowski-Kordesch*, 2010].

### 4.2. The Upper Member

#### 4.2.1. Description

The association characterizing the upper part of section B and sections C and D (Figure 2) comprises predominantly red, poorly sorted, clast- and matrix-supported conglomerates (facies Gcm and Gmm) with intercalated mudrocks (facies Fm and Fsm) (Figures 3d to 3f). Conglomerate beds are massive and disorganized, with mostly angular to subangular pebbles and cobbles. Clast-supported conglomerate beds of Facies Gcm, generally tens of cm to 2-m thick, are laterally discontinuous and may display erosional base. Matrix between gravels is muddy sands, and clast imbrication was never observed in this facies. Matrix-supported conglomerates of Facies Gmm consists of pebbles, cobbles, and locally boulders set

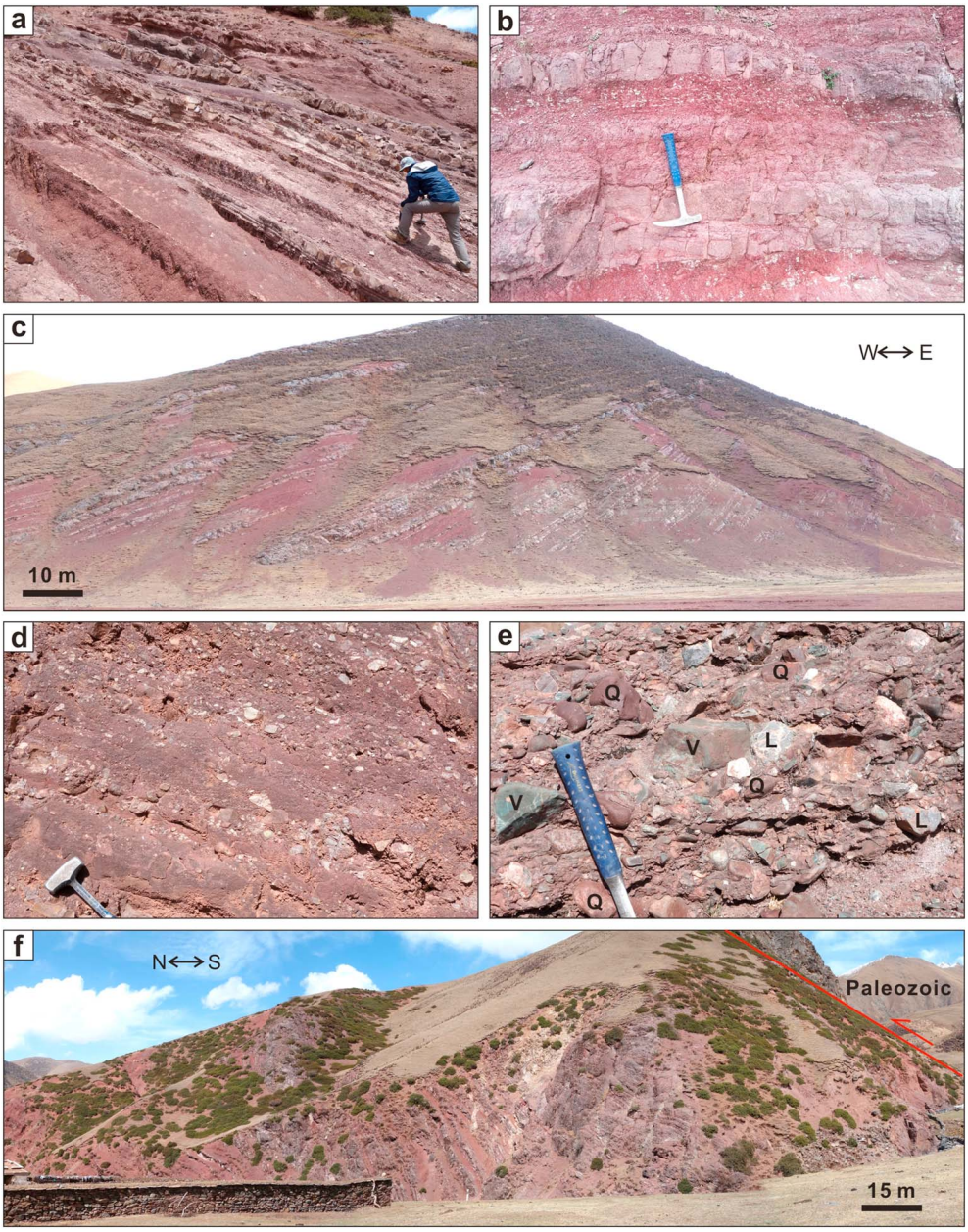


**Figure 3.** Field photographs of the Damxung Conglomerate. (a) Red lenticular sandstone beds and mudrocks in section A; (b) Sandstone beds with cross-lamination interbedded with red mudrocks with caliche nodules in the lower part of section B; (c) Panorama of section B, showing upward (westward) thicken of the sandstone beds; (d) Matrix-supported conglomerate from section C; (e) Clast-supported conglomerate from section D; Q, quartz sandstone; L, limestone; V, volcanic clasts; (f) Panorama of the section B, showing conglomerate beds atop the Damxung Conglomerate, tectonically overlain by Paleozoic strata along the north-directed Damxung thrust.

in a muddy or sandy mud-matrix. Bed thickness varies from ~20 cm to ~2 m. Amalgamated beds lacking internal structure may be stacked to form several tens of m-thick intervals. Pebbly sandstones (facies Sm) interbedded with conglomerates are subordinate. Mudrocks of Facies Fm and Fsm contain rare carbonate nodules.

#### 4.2.2. Interpretation

The lithofacies association is interpreted as deposited in a proximal alluvial-fan setting. Clast-supported pebble to cobble conglomerates (lithofacies Gcm) are interpreted to have been deposited by flows with

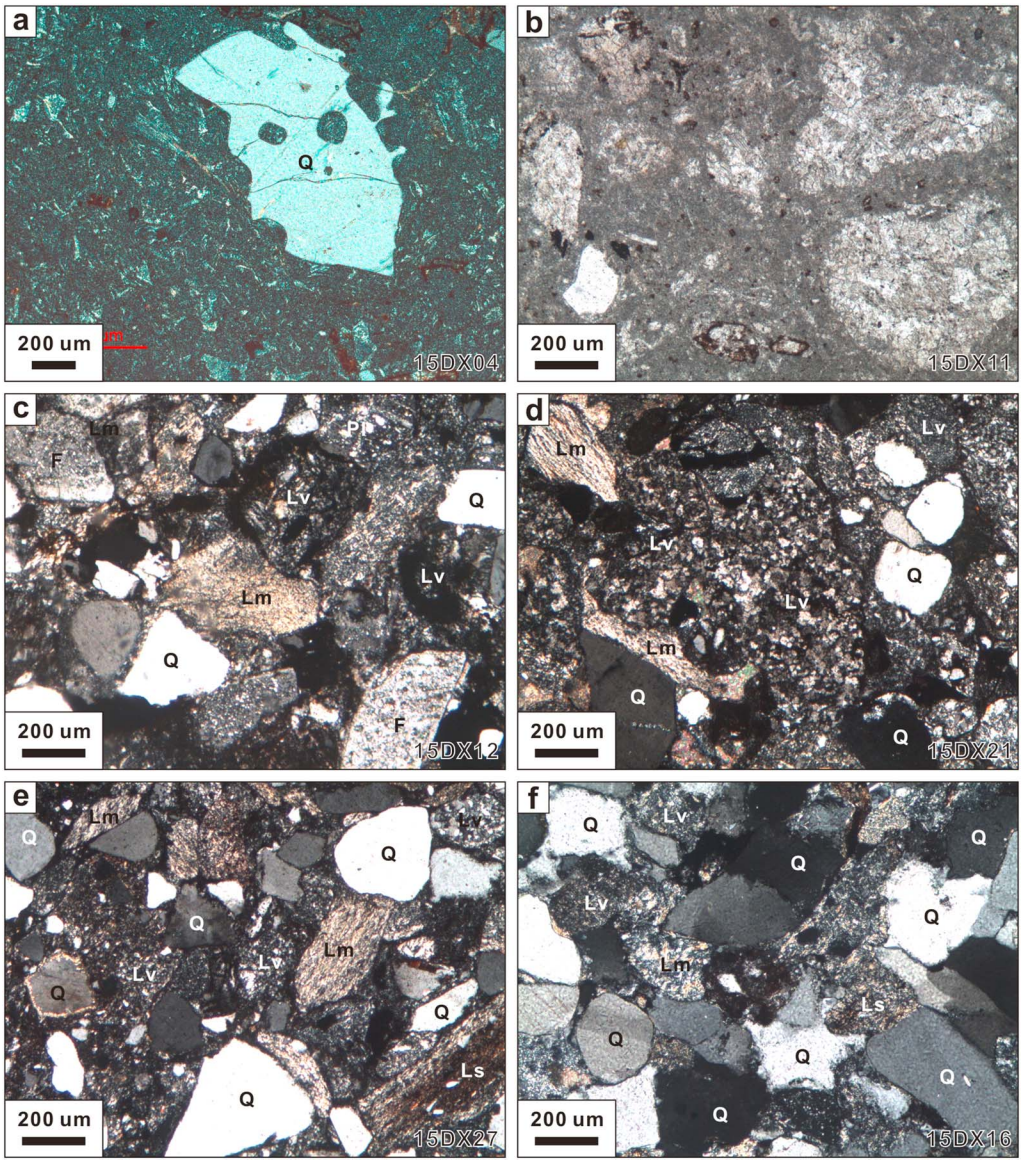


**Figure 4.** Petrography of the Damxung Conglomerate. (a and b) Felsic tuff and biomicrite from the base the unit; (c to f) Sandstone samples, showing progressive increase up-section in quartz (Q) and sedimentary/metasedimentary rock fragments (Ls, Lm) at the expense of volcanic rock fragments (Lv; F = Feldspar).

high sediment concentrations, possibly flash floods [*Sun et al.*, 2015]. Disorganized, matrix-supported conglomerates (lithofacies Gmm) including those with boulder clasts suggest deposition by plastic and/or pseudoplastic debris flows [*Blair and McPherson*, 1994]. The interlayered lenticular sandstones (Facies Sm) and mudrocks (Facies Fsm and Fm) represent waning debris-flow deposits.

## 5. Chronostratigraphy

U–Pb dating of zircon crystals extracted from tuff layers intercalated at the base of the Damxung Formation provides a direct constraint on depositional age. Two tuff samples from section A yielded ages of 111.1 ± 1.3 Ma (15DX04, $n$ = 18, 2σ) and 110.9 ± 1.3 Ma (15DX10, $n$ = 19, 2σ), respectively (Figure 5). This age is consistent with the youngest group of detrital zircons, yielding ages clustering between 120 and 110 Ma (Table S1). The entire Damxung Conglomerate may thus have been deposited during the earliest Albian, also considering the high accumulation rate typical of alluvial-fan environments.

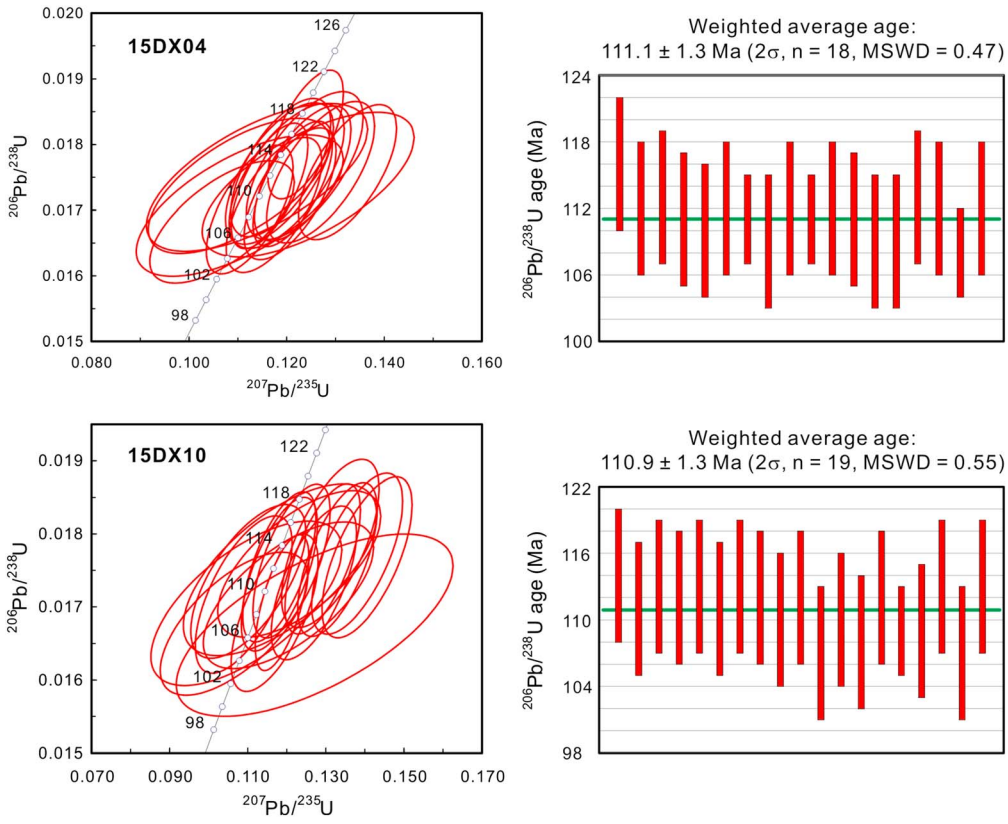


**Figure 5.** Concordia diagrams and weighted average U–Pb ages of zircon crystals from tuffs intercalated at the base of the Damxung Conglomerate.

### 5.1. Younger Conglomerate Units in the Damxung Area

Red conglomerate outcrops also occur in the Lagen La area north of Damxung and near the road to Nam Co [Lagen La Conglomerate of *Pullen et al.* [2008]], which were dated as early Eocene by the U–Pb zircon age of interbedded tuffs [*Kapp et al.*, 2007b] (Figure 1c). *Pullen et al.* [2008] mapped the Lagen La Conglomerate and the Damxung Conglomerate as a single unit, and thus suggested prolonged deposition of continental red beds in the Damxung area from the Cretaceous to the Eocene. The Lagen La Conglomerate, however, contains mainly pebbles to boulders of Aptian–Albian limestones [*Kapp et al.*, 2007b]. Such marked differences in composition (see the clastic composition of the Damxung Conglomerate below) and depositional ages indicate that the Lagen La Conglomerate was a much younger clastic unit probably formed as a result of India-Asia collision initiated in the Middle Paleocene [*Hu et al.*, 2015].

## 6. Provenance Data and Interpretation

### 6.1. Paleocurrents and Sediment Composition

A few paleocurrent directions measured from trough cross-laminations in the lower part of the Damxung Conglomerate indicate southward to southeastward sediment transport (Figure 2), suggesting a sedimentary source to the north of the depositional site. Pebbles and cobbles are all volcanic rocks in the lower part of the unit, whereas clasts of quartz sandstones prevail over volcanic rocks and minor limestones and granitoids in the upper part (Figure 2). Detrital modes of sandstones evolve up-section from lithic to quartzo-lithic and eventually litho-quartzose (Figures 4c to 4f and 6a). Volcanic lithics, representing >90% of the bulk sediment at the base of the unit, decrease progressively upward to represent only ~13% of total grains at the top of the unit. Conversely, sedimentary/metasedimentary rock fragments and monocrystalline quartz increase up-section from 0% to ~45% and from 7% to ~58% of total grains, respectively (Figure 6). Quartz grains are mostly rounded to subrounded, suggesting a recycled origin, but a few display sharp corners and

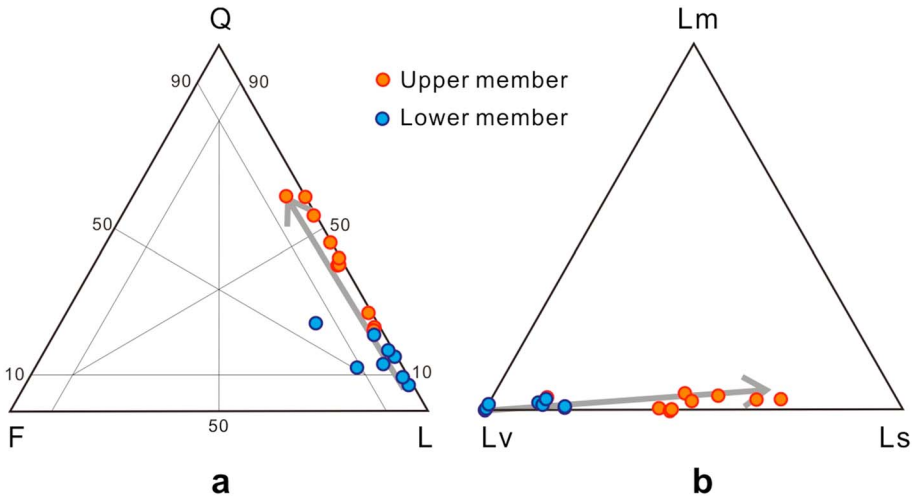


**Figure 6.** Sandstone petrography. Arrows in the ternary diagrams outline the steady compositional trend from base to top of the unit. Q, quartz; F, feldspar; L, total lithic fragments; Lm, metamorphic; Ls, sedimentary; Lv, volcanic.

embayments suggesting a felsic volcanic source. Feldspars are few (0 to 15%) throughout the unit and decrease up-section.

### 6.2. Age and Isotopic Signatures of Detrital Zircons

Age spectra of detrital zircons from the Damxung Conglomerate display an Early Cretaceous peak and older ages ranging from ~0.5 to ~3 Ga (Figure 7). Similar results were obtained by *Pullen et al.* [2008]. Early Cretaceous ages cluster between ~110 and 120 Ma; ages around 130 Ma also occur in sample 15DX15 collected from the top of the unit. Older ages show a major cluster at ~500–600 Ma (peak at ~515 Ma), and additional clusters at 900–1300 Ma, 1600–1900 Ma and 2400–2600 Ma. The proportion of Early Cretaceous ages decreases up-section from 96% to ~25%; pre-Mesozoic ages conversely increase.

The $\varepsilon_{Hf}(t)$ values of Early Cretaceous zircons range mostly between −15 and +1, corresponding to crustal model ages ($T_{DM}^{C}$) of ~1.2–2.0 Ga. Pre-Mesozoic zircons show $\varepsilon_{Hf}(t)$ values ranging widely from −30 to +10, corresponding to crustal model ages ($T_{DM}^{C}$) between 1.0 and 3.5 Ga. Zircon crystals from the two tuff samples yielded similar Hf isotopes as detrital zircons with Early Cretaceous ages (Figure 8).

### 6.3. Interpretations

The presence of tuffs and the abundance of volcanic clasts in the Damxung Conglomerate indicate dominant supply from a nearby active volcanic source. Penecontemporaneous volcanic activity is confirmed by the youngest U–Pb ages of detrital zircons in interlayered sandstones, which are close to the age of zircon crystals in tuff layers (Figure 7). The volcanic source can be identified reliably by the Hf isotope signature of detrital zircons, because igneous rocks in the South and North Lhasa subterranes have different isotopic features [*Zhu et al.*, 2011a; *Hou et al.*, 2015]. The South Lhasa (Gangdese) magmatic belt yields predominantly zircons with positive $\varepsilon_{Hf}(t)$ values [*Chu et al.,* 2006; *Ji et al.*, 2009], whereas the North Lhasa magmatic belt is characterized by zircons mainly with negative $\varepsilon_{Hf}(t)$ values [*Chiu et al.*, 2009; *Zhu et al.*, 2011a] (Figure 8). Detrital zircons from the Damxung Conglomerate yielding Early Cretaceous ages have mainly negative to slightly positive $\varepsilon_{Hf}(t)$ values (−15 to +1), matching the signature of the North Lhasa subterrane (Figure 8). Moreover, ages cluster between ~120 and 110 Ma, matching the age of the North Lhasa magmatic flare up [at 113 ± 5 Ma; [*Zhu et al.*, 2011a]]. We thus conclude that the Lower Cretaceous volcanic rocks [the Zenong Group volcanic rocks, Figure 1b; *Zhu et al.*, 2011a] in North Lhasa subterrane is the source of the volcanic detritus in the Damxung Conglomerate. A northerly provenance is confirmed by the paleocurrent directions which are southward to southeastward. Zircon with similar ages and Hf isotopes were also reported in the Banggong-Nujiang suture zone farther north [e.g., *Kapp et al.*, 2007a; *Zhu et al.*, 2016]. The proximal alluvial fan facies of the Damxung Conglomerate, however, suggests us to consider the Bangong-Nujiang suture zone, located 300 km far to the north, as an unlikely source.

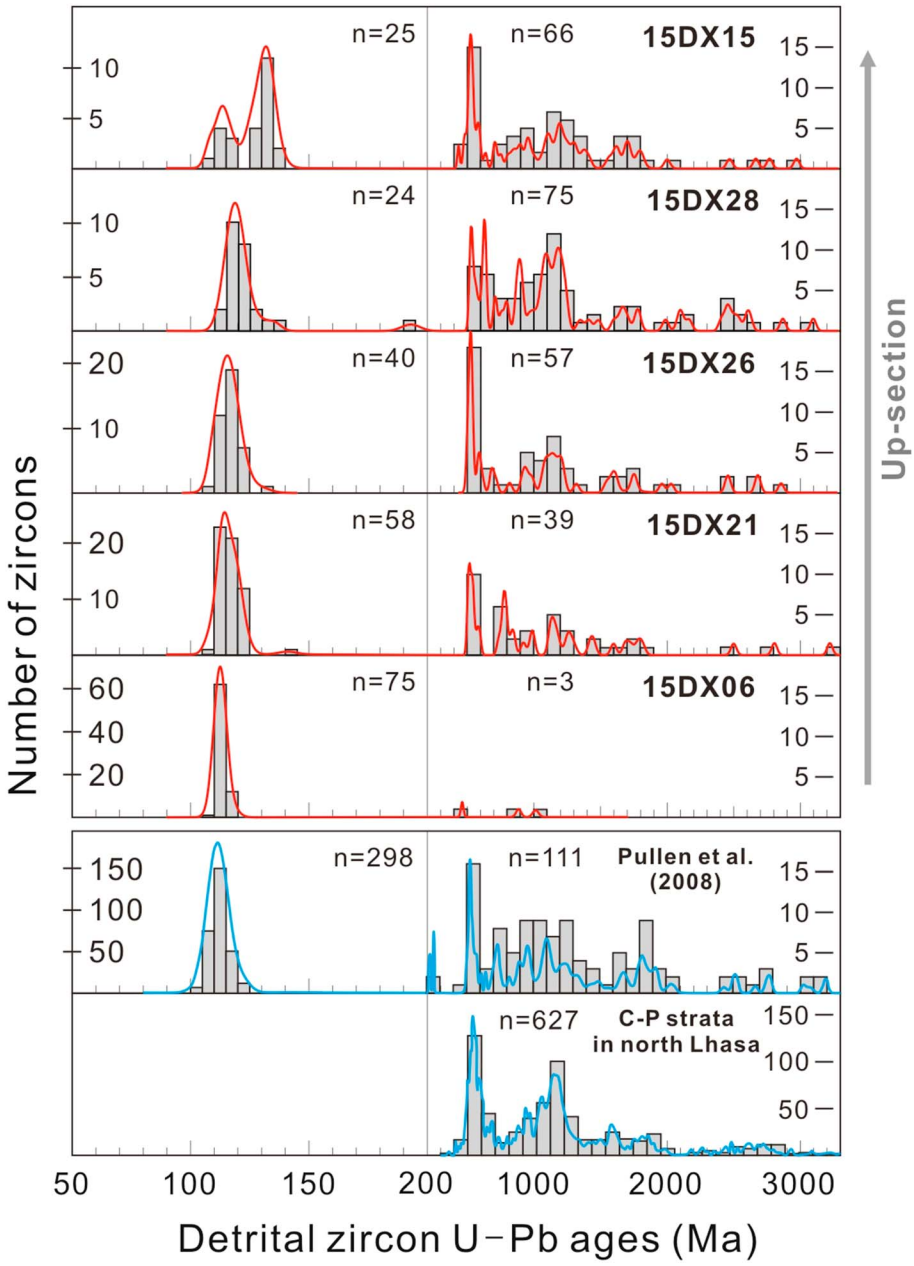


**Figure 7.** U–Pb age-frequency plot for detrital zircons from the Damxung Conglomerate. Published ages from Damxung Conglomerate [*Pullen et al.*, 2008] and Carboniferous–Permian strata in the Lhasa terrane [*Leier et al.*, 2007c; *Pullen et al.*, 2008; *Zhu et al.*, 2011b] are shown for comparison. Note the change in scale along the x-axis.

Quartz sandstone, limestone and slate rock fragments, together with zircon grains yielding Early Paleozoic–Precambrian ages, indicate recycling of (meta)sedimentary parent rocks (Figures 4c to 4f). Paleozoic strata, which are widely exposed nearby and include all of these lithologies, are interpreted as the source of recycled detritus (Figure 1c). U–Pb age spectra and Hf isotopic values of detrital zircons in these Paleozoic strata [*Leier et al.*, 2007c; *Pullen et al.*, 2008; *Zhu et al.*, 2011b] compare well with those of detrital zircons yielding Early Paleozoic to Precambrian ages from the Damxung Conglomerate (Figures 7 and 8), which supports our interpretation.

Detrital modes and U–Pb age spectra of detrital zircons reveal an evident progressive provenance change from the base to the top of the Damxung Conglomerate. Volcanic rock fragments and detrital zircons yielding Early Cretaceous ages gradually decrease up-section, whereas sedimentary to very-low-grade

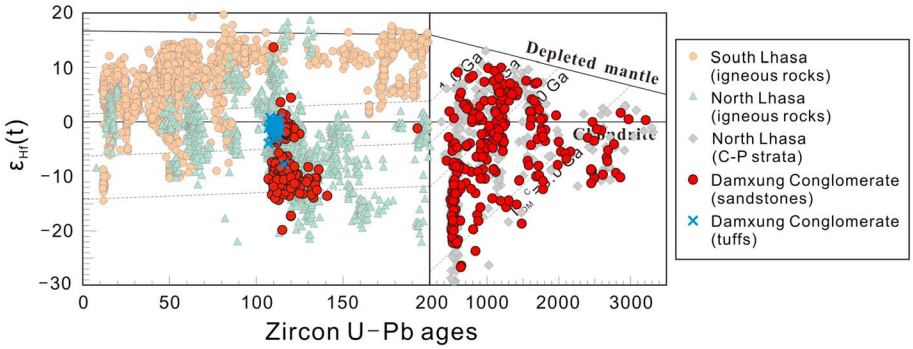


**Figure 8.** U–Pb age vs. $\varepsilon_{Hf}(t)$ plot of detrital zircons from the Damxung Conglomerate. Data from igneous rocks of the South and North Lhasa subterranes [*Hou et al*., 2015], Carboniferous–Permian sandstones [*Zhu et al*., 2011b] and tuffs interbedded in the Damxung Conglomerate are plotted for comparison.

metasedimentary rock fragments, quartz grains, and Early Paleozoic-Precambrian ages of detrital zircons correspondingly increase (Figure 9). Such a clear trend testifies to progressive erosional unroofing of the source area (Figure 10). Lower Cretaceous volcanic rocks [i.e., the Zenong Group; [*Zhu et al*., 2011a]], representing the uppermost stratigraphic level in the source, were eroded first, supplying overwhelming volcanic detritus during initial deposition of the Damxung Conglomerate. As erosional denudation continued, the underlying Paleozoic strata were gradually exhumed, and detritus recycled from sedimentary to very-low-grade metasedimentary rocks increased with time. Similar compositional trends associated with progressive erosional unroofing of source rocks are commonly observed in syn-tectonic conglomerate units, such as the Upper Cretaceous Echo Canyon Conglomerate in northeastern Utah of USA [*DeCelles*, 1988].

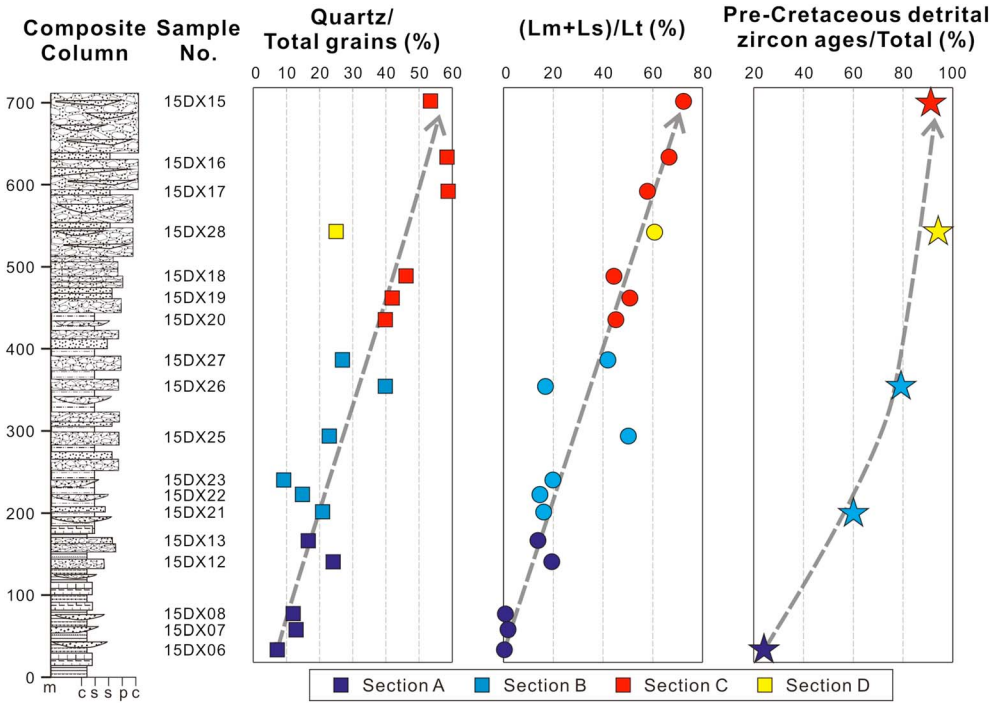


**Figure 9.** Changes in sandstone petrography and ages of detrital zircons throughout the Damxung Conglomerate. Detritus recycled from Paleozoic (meta)sedimentary strata increase up-section whereas volcanic detritus and penecontemporaneous zircon grains decrease. Such systematic trend is interpreted to reflect progressive erosional unroofing of the source area.

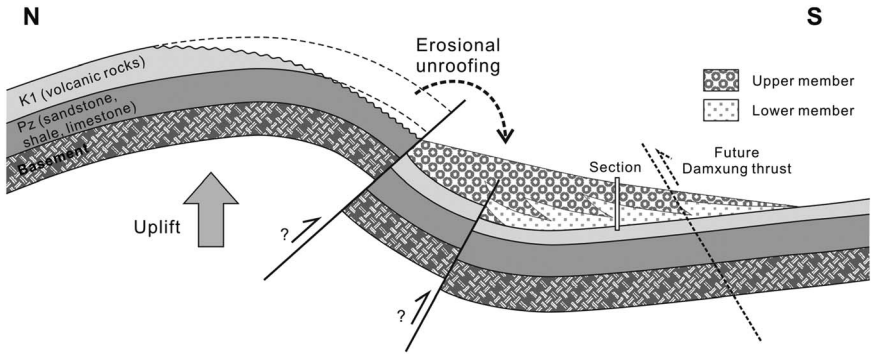


**Figure 10.** Schematic diagram illustrating control by progressive unroofing of the source on compositional trends observed throughout the Damxung Conglomerate.

## 7. Discussion

### 7.1. Depositional Model for the Damxung Conglomerate

Sedimentology of the Damxung Conglomerate suggests rapid deposition in braided-rivers and alluvial fans proximal to the source area. The coarse-grained texture, the upward-coarsening clastic size and the progressive compositional change from the base to the top point to a syn-tectonic origin of the strata. Deposition of the Damxung Conglomerate could be subdivided into two continuous stages through sedimentary facies and provenance results (Figure 10). During the early stage of deposition, sediments were relatively fine-grained, deposited in distal alluvial fan to braidplain environments, and consist of mainly volcanic detritus. The sedimentary characteristics indicate a low relief in the source area or a far distance from the source to the basin, and sediments were eroded from the very surface penecontemporaneous volcanic rocks. The presence of bioclastic limestone beds at the base indicates that during initial deposition of the Damxung Conglomerate the sedimentary basin was close to, and temporarily even below sea-level. Sediments of the late stage comprise coarse-grained conglomerates that were deposited in a proximal alluvial-fan setting, indicating a progressive increase in relief of the nearby source areas, enough to generate debris flows during intense precipitation events. The presence of abundant recycled detritus indicates erosional exhumation of sedimentary/metasedimentary basement rocks. Therefore, the Damxung Conglomerate documented a phase of significant topographic growth and erosion of the North Lhasa subterrane.

Sedimentary characteristics of the Damxung Conglomerate are similar to these of the foreland deposits related to thrust belts [e.g., *DeCelles*, 1988; *Wang et al.*, 2013]. Early Cretaceous thrusts have been identified in the middle-western part of North Lhasa subterrane, neighboring the Bangong-Nujiang suture zone [e.g., *Kapp et al.*, 2003, 2007a], but the eastward prolongation of these thrust were not well constrained. Southward thrust has been observed in the Nam Co area (i.e., the south Nam Co thrust) north of the Damxung Conglomerate, but it was interpreted as a Cenozoic structure [*Pullen et al.*, 2008]. Therefore, detailed structure analyses on the North Lhasa subterrane is still needed in the future work to reveal the coupling relationship between the tectonics in the source area and deposition of the Damxung Conglomerate.

### 7.2. Early Cretaceous Topographic Growth and Paleogeography of the Lhasa Terrane

Deposition of the Damxung Conglomerate indicates a phase of significant topographic growth and erosion on the North Lhasa subterrane. The timing of this event is constrained precisely by zircon U–Pb dating of interlayered tuffs to have occurred at ~111 Ma. In order to establish whether this episode was of only local or of broader regional significance, we can compare our results from the Damxung area with the stratigraphic records of the Linzhou basin, located in the eastern part of the South Lhasa subterrane, and of the Xigaze forearc basin, located to the south of the Gangdese arc (Figure 1a).

The youngest marine strata in the Linzhou basin are the *Orbitolinid*-bearing limestones with interbedded siltstones of the Penbo Member of the Takena Formation, overlain conformably by red mudrocks, sandstones and conglomerates of the Lhunzhub member of the Takena Formation (Figure 11a). The Penbo member was deposited in a low-energy shallow-marine environment, whereas the Lhunzhub member in a fluvial environment [*Leier et al.*, 2007a]. The timing of transition from marine to continental sedimentation is

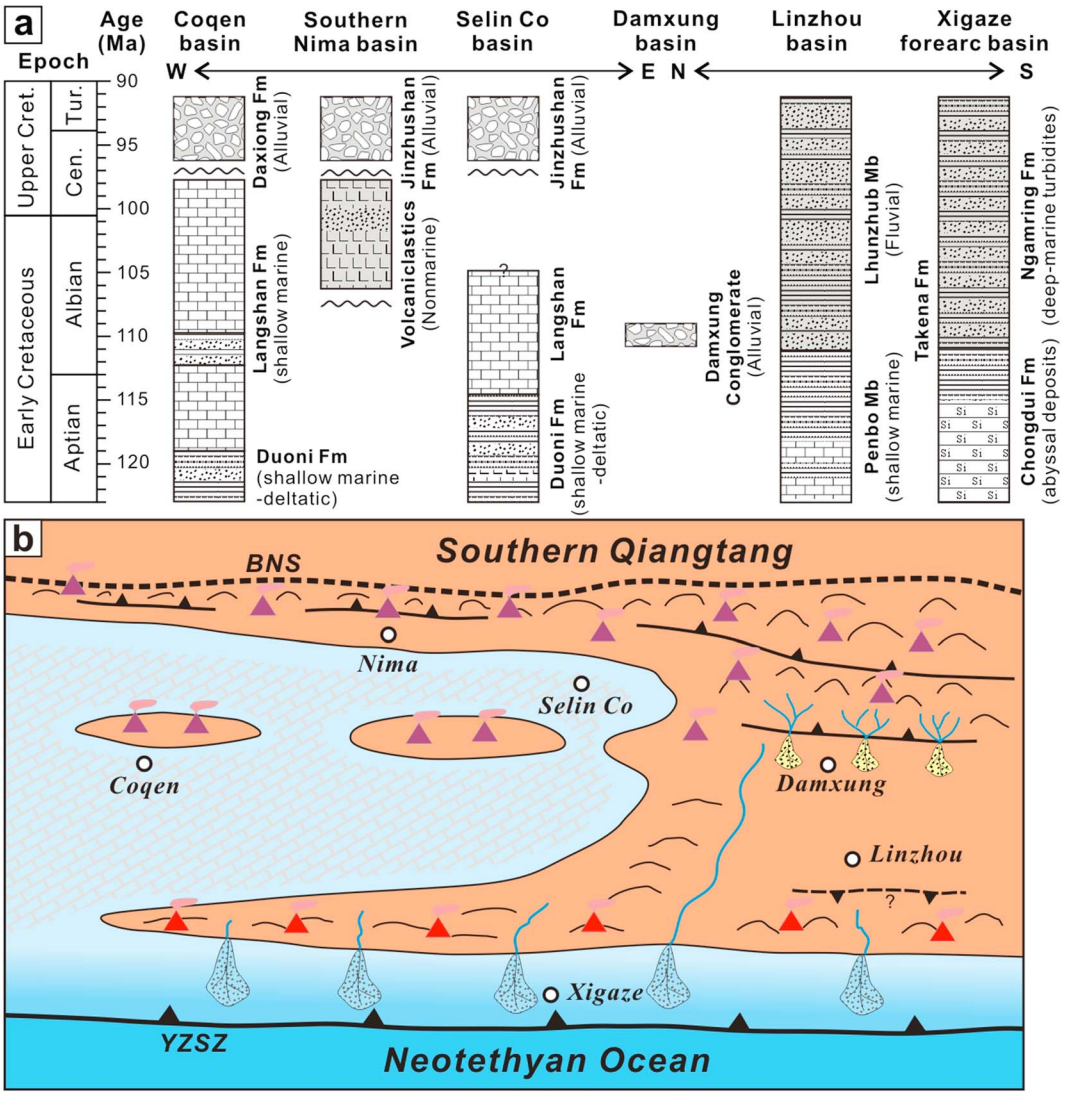


**Figure 11.** (a) Stratigraphic and facies comparison among principal Cretaceous basins on the Lhasa terrane. Sources of stratigraphic data: Coqen basin [*Sun*, 2015*; Sun et al.*, 2015]; Southern Nima basin [*DeCelles, et al.*, 2007a*; Kapp et al.*, 2007a]; Selin Co basin [*Zhang et al.*, 2011]; Xigaze forearc basin [*Dai et al.*, 2015; *Orme and Laskowski*, 2016; *Wang et al.*, 2017]; Linzhou basin [*Leier et al.*, 2007a*; Boudagher-Fadel et al.*, 2017]. (b) Paleogeographic sketch map of the Lhasa terrane at 110 Ma, showing westward retreat of seaways and diachronous uplift of the Lhasa terrane from east to west. BNS, Bangong-Nujiang suture; YZSZ, Yarlung-Zangbo subduction zone.

constrained as younger than the early Aptian *orbitolinid* assemblage found in the Penbo Member [*Boudagher-Fadel et al.*, 2017] and as broadly coeval to the youngest detrital zircon grains from the base of the Lhunzhub member which yielded U–Pb ages of ~114–110 Ma [Sample PENBO1; [*Leier et al.*, 2007c]]. Such an age is approximately equivalent to that of the base of the Damxung Conglomerate. Red bed sedimentation may have thus begun roughly at the same time in the Damxung area and in the Linzhou basin. The volcaniclastic sandstones of the Lhunzhub Member were interpreted as derived from the Gangdese arc in the south [*Leier et al.*, 2007a], but supply from the North Lhasa subterrane is possible, because the Lhunzhub member contains many zircon grains yielding Early Paleozoic to Precambrian ages [*Leier et al.*, 2007c]. Such old zircons are quite rare in the Gangdese arc.

In the Xigaze forearc basin, deep-sea turbidites were deposited directly above the red chert and siliceous shales representing the sedimentary cover of the Yarlung-Zangbo ophiolites [*Girardeau et al.*, 1984; *Einsele et al.*, 1994; *Wang et al.*, 2012] (Figure 11a). The onset of clastic sedimentation in the forearc basin, constrained precisely at 113–110 Ma by zircon U–Pb dating of intercalated tuff layers [*Dai et al.*, 2015; *Orme and Laskowski*,

2016], was considered as a result of initial topographic growth on the Lhasa terrane [*Wang et al.*, 2017]. Sandstones from the base of the Xigaze forearc-basin succession contain sediments derived from both Gangdese arc and North Lhasa subterrane, indicating that the Gangdese belt was emerged but still at a low elevation, and that the river system feeding the Xigaze forearc basin had its source in the North Lhasa subterrane [*Dai et al.*, 2015; *Orme and Laskowski*, 2016; *Wang et al.*, 2017].

Early Cretaceous topographic growth on the Tibetan plateau is also supported by the stratigraphic record of sedimentary basins located on the North Lhasa subterrane near the Bangong-Nujiang suture. In the southern Nima basin, the oldest non-marine strata are represented by volcanic rocks and volcaniclastic conglomerates and sandstones overlying unconformably Jurassic to the lowermost Cretaceous marine clastic rocks [*Kapp et al.*, 2007a; *DeCelles et al.*, 2007]. U–Pb ages of zircons from a volcaniclastic sandstone bed yielded an age of 106 ± 2 Ma [*Kapp et al.*, 2007a], which provides a minimum age constraint for initial uplift around the Nima basin.

Our sedimentary facies, provenance and chronostratigraphic data from the Damxung Conglomerate and its comparison with the coeval strata in the adjacent regions indicate that significant rocks uplift and exhumation have occurred on the Lhasa terrane in the Early Cretaceous (early Albian) Time. We emphasize, however, that the data we present cannot constrain the absolute amount of surface uplift. Paleoaltimetry study is still needed to quantify the Early Cretaceous geomorphy on the Lhasa terrane.

In contrast to the widespread continental facies deposition on the eastern part of the Lhasa terrane, shallow-marine limestones and volcaniclastic rocks were deposited in the central-western part of the Lhasa terrane during the Early Cretaceous [*Zhang et al.*, 2011; *Sun et al.*, 2015]. Marine strata represented by limestones of the Langshan Formation accumulated until the early Albian at least in the Selin Co basin, where topographic uplift is documented at a stage later than in the Damxung area by Upper Cretaceous alluvial-fan conglomerates of the Jingzhushan Formation [*Zhang et al.*, 2011]. In the Coqen basin farther west, the Langshan Formation continued to be deposited until the early Cenomanian [*Sun et al.*, 2015; *Boudagher-Fadel et al.*, 2017], and was overlain unconformably by conglomerates of the Daxiong Formation deposited between ~96 and ~91 Ma and documenting initial topographic growth around this area at that time. Therefore, the sea retreat and initial topographic growth on the Lhasa terrane were diachronous, progressive roughly from east to west (Figure 11a). The northernmost, eastern and southern parts of the Lhasa terrane began to emerge from the sea between latest Aptian and earliest Albian times, whereas the western Lhasa terrane remained covered by a shallow marine until the early Cenomanian (Figure 11b).

### 7.3. Geodynamic Implications

Two geodynamic processes may have induced topographic growth on the Lhasa terrane during the late Early Cretaceous: collision between the Qiangtang and Lhasa terranes [*Murphy et al.*, 1997; *P. Kapp et al.*, 2005; *Sun et al.*, 2015], or northward subduction of Neotethyan oceanic lithosphere beneath the Lhasa terrane [*Leier et al.*, 2007a; *Kapp et al.*, 2007b]. *Pullen et al.* [2008] interpreted the Damxung Conglomerate as deposited in the Gangdese retroarc foreland basin, because the unit is exposed in the footwall of the north-directed Damxung thrust, and because volcanic detritus was interpreted as derived from the Gangdese magmatic arc in the south. In their model, deposition of the Damxung Conglomerate was thus controlled by subduction of Neotethyan oceanic lithosphere and development of Gangdese retroarc thrusts. In contrast, our provenance results indicate that the Damxung Conglomerate was derived instead from the North Lhasa subterrane in the north. Consequently, we associate deposition of the Damxung Conglomerate with geodynamic processes related to the collision between the Lhasa and Qiangtang terranes in the north rather than to Neothyan subduction in the south. The Damxung thrust is interpreted as a later tectonic feature that juxtaposed Paleozoic strata onto the previously deposited Damxung Conglomerate.

Although the timing of the Qiangtang-Lhasa collision is poorly constrained, it has long been established that it took place between the Late Jurassic and the Early Cretaceous [*Allègre et al.*, 1984; *Marcoux et al.*, 1987; *Dewey et al.*, 1988; *P. Kapp et al.*, 2005]. Early Cretaceous deformation and exhumation as a result of Lhasa-Qiangtang collision have been widely documented in the Bangong-Nujiang suture zone, and were interpreted as a result of Lhasa-Qiangtang collision [*P. Kapp et al.*, 2005; *Kapp et al.*, 2007a; *Guynn et al.*, 2006]. Crustal-thickening induced by the collision-related fold and thrust was therefore the most possible mechanism for the Early Cretaceous uplift and exhumation of the North Lhasa subterrane (Figure 11b).

Geochronological studies of magmatic rocks in the North Lhasa subterrane and along the Bangong-Nujiang suture have revealed an Early Cretaceous magmatic flare up at 113 ± 5 Ma [*Zhu et al.*, 2011a; *Chen et al.*, 2014]. Such explosive magmatic eruptions have been tentatively ascribed to breakoff of the Bangong–Nujiang oceanic slab following the Qiangtang-Lhasa collision [*Zhu et al.*, 2011a; *Hou et al.*, 2015]. The coincidence in time between the North Lhasa magmatic flare up and initial topographic growth on the Lhasa terrane suggests the possibility of a causal link. Crustal shortening, tectonic uplift, and topographic growth of the Bangong-Nujiang suture belt and North Lhasa subterrane may have followed the transition from "soft" to "hard" collision between the Qiangtang and Lhasa terranes.

The welding between the Qiangtang and Lhasa terranes and the reduction in convergence rate between them may have led to a progressive increase in compressive stress induced by the northward subduction of the Neotethyan slab in the south. Consequently, crustal thickening of the South Lhasa subterrane may have initiated topographic growth of the Gangdese arc and accelerated its erosion, fostering clastic sedimentation and progressive filling of the Xigaze forearc basin [*Wang et al.*, 2017].

We suggest that geodynamic processes associated to ongoing collision between the Lhasa and Qiantang terranes along the Bangong–Nujiang suture represented the principal tectonic control on initial uplift of the Lhasa terrane around 111 Ma. The gradual westward retreat of seaways and diachronous topographic growth from east to west might have been controlled either by oblique convergence along the Bangong–Nujiang suture and/or by inherited geological and topographic features of the Lhasa terrane.

## 8. Conclusions

The Damxung Conglomerate testifies to deposition in braidplain-distal alluvial-fan environment passing upward to proximal alluvial-fan settings during the earliest Albian time. Paleocurrents, sandstone petrography and zircon ages and Hf isotopes concur to indicate clastic supply from the North Lhasa terrane, where penecontemporaneous volcanic rocks were eroded first, and their Paleozoic sedimentary/metasedimentary substratum progressively exhumed later on. Deposition of the Damxung Conglomerate testifies to initial topographic growth in the North Lhasa source region, which began at 111 Ma as precisely constrained by U–Pb dating of zircon crystal in tuff layers intercalated at the base of the unit.

The tectonic uplift phase documented by the Damxung Conglomerate coincides in time with transition from shallow-marine to continental red bed deposition in the Linzhou basin and with the onset of clastic deposition by turbidity currents in the Xigaze forearc basin. The initial topographic growth on the eastern Lhasa terrane thus determined a radical paleogeographic change in southern Tibet at that time. Marine sedimentation persisted for another 10–15 Ma in the Coqen basin of the western Lhasa terrane, indicating diachronous topographic growth and sea retreat from east to west across the Lhasa tectonic domain.

**Acknowledgments**
The data supporting this paper are available as supporting information. We thank Yue-Heng Yang for help during zircon U–Pb dating and Hf isotopic analyses. We are deeply grateful to the editor Paul Tregoning, the reviewer Andrew Leier and an anonymous reviewer for their constructive comments. This work was financially supported by the National Key R&D Program of China (2016YFC0600407), the National Science Foundation of China (projects 41672109, 41472081) and the China Geological Survey Project (DD20160022-01).

## References

An, W., X. M. Hu, E. Garzanti, M. K. BouDagher-Fadel, J. G. Wang, and G. Y. Sun (2014), Xigaze forearc basin revisited (South Tibet): Provenance changes and origin of the Xigaze ophiolite, *Geol. Soc. Am. Bull.*, *126*(11–12), 1595–1613, doi:10.1130/B31020.1.

An, Z. S., J. E. Kutzbach, W. L. Prell, and S. C. Porter (2001), Evolution of Asian monsoons and phased uplift of the Himalaya–Tibetan plateau since late Miocene times, *Nature*, *411*(6833), 62–66, doi:10.1038/35075035.

Andersen, T. (2002), Correction of common lead in U–Pb analyses that do not report $^{204}$Pb, *Chem. Geol.*, *192*(1–2), 59–79, doi:10.1016/S0009-2541(02)00195-X.

Allègre, C. J., et al. (1984), Structure and evolution of the Himalayan-Tibet orogenic belt, *Nature*, *307*, 17–22, doi:10.1038/307017a0.

Blair, T. C., and J. G. McPherson (1994), Alluvial fans and their natural distinction from rivers based on morphology, hydraulic processes, sedimentary processes, and facies assemblages, *J. Sediment. Res.*, *64*(3), 450–489, doi:10.1306/D4267DDE-2B26-11D7-8648000102C1865D.

BlichertToft, J., and F. Albarède (1997), The Lu–Hf isotope geochemistry of chondrites and the evolution of the mantle–crust system, *Earth Planet. Sci. Lett.*, *148*(1–2), 243–258, doi:10.1016/S0012-821X(97)00040-X.

Boudagher-Fadel, M. K., X. M. Hu, G. D. Prince, G. Y. Sun, J. G. Wang, and W. An (2017), Foraminiferal biostratigraphy and paleoenvironmental analysis of the mid-cretaceous limestones in the southern Tibetan plateau, *J. Foraminiferal Res.*, *47*(2), 188–207.

Chen, Y., D. C. Zhu, Z. D. Zhao, F. Y. Meng, Q. Wang, M. Santosh, L. Q. Wang, G. C. Dong, and X. X. Mo (2014), Slab breakoff triggered ca. 113 ma magmatism around Xainza area of the Lhasa terrane, Tibet, *Gondwana Res.*, *26*(2), 449–463, doi:10.1016/j.gr.2013.06.005.

Chiu, H. Y., S. L. Chung, F. Y. Wu, D. Y. Liu, Y. H. Liang, I. J. Lin, Y. Iizuka, L. W. Xie, Y. B. Wang, and M. F. Chu (2009), Zircon U–Pb and Hf isotopic constraints from eastern Transhimalayan batholiths on the precollisional magmatic and tectonic evolution in southern Tibet, *Tectonophysics*, *477*(1–2), 3–19, doi:10.1016/j.tecto.2009.02.034.

Chu, M. F., S. L. Chung, B. A. Song, D. Y. Liu, S. Y. O'Reilly, N. J. Pearson, J. Q. Ji, and D. J. Wen (2006), Zircon U–Pb and Hf isotope constraints on the Mesozoic tectonics and crustal evolution of southern Tibet, *Geology*, *34*(9), 745–748, doi:10.1130/022725.1.

Dai, J. G., C. S. Wang, D. C. Zhu, Y. L. Li, H. T. Zhong, and Y. K. Ge (2015), Multi-stage volcanic activities and geodynamic evolution of the Lhasa terrane during the cretaceous: Insights from the Xigaze forearc basin, *Lithos*, *218–219*, 127–140, doi:10.1016/j.lithos.2015.01.019.

DeCelles, P. G. (1988), Lithologic provenance modeling applied to the late cretaceous Synorogenic Echo canyon conglomerate, Utah: A case of multiple source areas, *Geology*, *16*(11), 1039–1043, doi:10.1130/0091-7613(1988)016<1039:LPMATT>2.3.CO;2.

DeCelles, P. G., R. P. Langford, and R. K. Schwartz (1983), Two new methods of paleocurrent determination from trough cross-stratification, *J. Sediment. Petrol.*, *53*(2), 629–642.

DeCelles, P. G., M. B. Gray, R. B. Cole, N. Pequera, D. A. Pivnik, K. D. Ridgway, and P. Srivastava (1991), Controls on synorogenic alluvial-fan architecture, Beartooth conglomerate (Palaeocene), Wyoming and Montana, *Sedimentology*, *38*, 567–590, doi:10.1111/j.1365-3091.1991.tb01009.x.

DeCelles, P. G., P. Kapp, L. Ding, and G. E. Gehrels (2007), Late cretaceous to mid-tertiary basin evolution in the central Tibetan plateau: Changing environments in response to tectonic partitioning, aridification, and regional elevation gain, *Geol. Soc. Am. Bull.*, *119*, 654–680, doi:10.1130/B26074.1.

Dewey, J. F., R. M. Shackleton, C. F. Chang, and Y. Y. Sun (1988), The tectonic evolution of the Tibetan plateau. Philosophical transactions of the Royal Society of London (series a), *Math. Phys. Sci.*, *327*, 379–413, doi:10.1098/rsta.1988.0135.

Einsele, G., et al. (1994), The Xigaze forearc basin: Evolution and facies architecture (cretaceous, Tibet), *Sediment. Geol.*, *90*, 1–32, doi:10.1016/0037-0738(94)90014-0.

Gierlowski-Kordesch, E. H. (2010), Lacustrine carbonates, in *Carbonates in Continental Settings: Facies, Environments and Processes*, *Dev. Sedimentol.*, edited by A. M. Alonso-Zarza and L. H. Tanner, vol. 61, pp. 1–101, Elsevier, Amsterdam.

Girardeau, J., J. Marcoux, and Y. G. Zao (1984), Lithologic and tectonic environment of the Xigaze ophiolite (Yarlung Zangbo suture zone, southern Tibet, China), and kinematics of its emplacement, *Eclogae Geol. Helv.*, *77*, 153–170.

Griffin, W. L., N. J. Pearson, E. Belousova, S. E. Jackson, E. van Achterbergh, S. Y. O'Reilly, and S. R. Shee (2000), The Hf isotope composition of cratonic mantle: LAM-MC-ICPMS analysis of zircon megacrysts in kimberlites, *Geochim. Cosmochim. Acta*, *64*(1), 133–147, doi:10.1016/S0016-7037(99)00343-9.

Griffin, W. L., X. Wang, S. E. Jackson, S. Y. O'Reilly, X. S. Xu, and X. M. Zhou (2002), Zircon chemistry and magma mixing, SE China: In-situ analysis of Hf isotopes, Tonglu and Pingtan igneous complexes, *Lithos*, *61*(3–4), 237–269, doi:10.1016/S0024-4937(02)00082-8.

Griffin, W. L., W. J. Powell, N. J. Pearson, and S. Y. O'Reilly (2008), GLITTER: Data reduction software for laser ablation ICP–MS, in *Laser Ablation–ICP–MS in the Earth Sciences: Current Practices and Outstanding Issues*, *Short Course Series*, vol. 40, edited by P. Sylvester, pp. 308–311, Mineralogical Association of Canada, Quebec.

Guynn, J. H., P. Kapp, A. Pullen, M. Heizler, G. E. Gehrels, and L. Ding (2006), Tibetan basement rocks near Amdo reveal "missing" Mesozoic tectonism along the Bangong suture, central Tibet, *Geology*, *34*, 505–508, doi:10.1130/G22453.1.

Harrison, T. M., P. Copeland, W. S. F. Kidd, and O. M. Lovera (1995), Activation of the Nyainqentanghla shear zone: Implications for uplift of the southern Tibetan plateau, *Tectonics*, *14*, 658–676, doi:10.1029/95TC00608.

He, S. D., P. Kapp, P. G. DeCelles, G. E. Gehrels, and M. Heizler (2007), Cretaceous–tertiary geology of the Gangdese arc in the Linzhou area, southern Tibet, *Tectonophysics*, *433*(1–4), 15–37, doi:10.1016/j.tecto.2007.01.005.

Hou, Z. Q., et al. (2015), Lithospheric architecture of the Lhasa terrane and its control on ore deposits in the Himalayan-Tibetan Orogen, *Econ. Geol.*, *110*, 1541–1575, doi:10.2113/econgeo.110.6.1541.

Hu, X. M., E. Garzanti, T. Moore, and I. Raffi (2015), Direct stratigraphic dating of India-Asia collision onset at the Selandian (middle Paleocene, 59 ± 1 ma), *Geology*, *43*(10), 859–862, doi:10.1130/G36872.1.

Ingersoll, R. V., T. F. Bullard, R. L. Ford, J. P. Grimm, J. D. Pickle, and S. W. Sares (1984), The effect of grain size on detrital modes: A test of the Gazi-Dickinson point-counting method, *J. Sediment. Petrol.*, *54*, 103–116, doi:10.1306/212F8783-2B24-11D7-8648000102C1865D.

Ji, W. Q., F. Y. Wu, S. L. Chung, J. X. Li, and C. Z. Liu (2009), Zircon U–Pb geochronology and Hf isotopic constraints on petrogenesis of the Gangdese batholith, southern Tibet, *Chem. Geol.*, *262*, 229–245, doi:10.1016/j.chemgeo.2009.01.020.

Kapp, J. L. D., T. M. Harrison, P. Kapp, M. Grove, O. M. Lovera, and L. Ding (2005), Nyainqentanglha Shan: A window into the tectonic, thermal, and geochemical evolution of the Lhasa block, southern Tibet, *J. Geophys. Res.*, *110*, B08413, doi:10.1029/2004JB003330.

Kapp, P., M. A. Murphy, A. Yin, T. M. Harrison, L. Ding, and J. Guo (2003), Mesozoic and Cenozoic tectonic evolution of the Shiquanhe area of western Tibet, *Tectonics*, *22*(4), 1029, doi:10.1029/2001TC001332.

Kapp, P., A. Yin, T. M. Harrison, and L. Ding (2005), Cretaceous-tertiary shortening, basin development, and volcanism in central Tibet, *Geol. Soc. Am. Bull.*, *117*, 865–878, doi:10.1130/B25595.1.

Kapp, P., P. G. DeCelles, G. E. Gehrels, M. Heizler, and L. Ding (2007a), Geological records of the Lhasa-Qiangtang and indo-Asian collisions in the Nima area of central Tibet, *Geol. Soc. Am. Bull.*, *119*, 917–933, doi:10.1130/B26033.1.

Kapp, P., P. G. DeCelles, A. L. Leier, J. M. Fabijanic, S. D. He, A. Pullen, and G. E. Gehrels (2007b), The Gangdese retroarc thrust belt revealed, *GSA Today*, *17*(7), 4–9, doi:10.1130/GSAT01707A.1.

Lee, H. Y., S. L. Chung, C. H. Lo, J. Q. Ji, T. Y. Lee, Q. Qian, and Q. Zhang (2009), Eocene Neotethyan slab breakoff in southern Tibet inferred from the Linzizong volcanic record, *Tectonophysics*, *477*, 20–35, doi:10.1016/j.tecto.2009.02.031.

Leier, A. L., P. G. DeCelles, P. Kapp, and L. Ding (2007a), The Takena formation of the Lhasa terrane, southern Tibet: The record of a late cretaceous retroarc foreland basin, *Geol. Soc. Am. Bull.*, *119*, 31–48, doi:10.1130/B25974.1.

Leier, A. L., P. G. DeCelles, P. Kapp, and G. E. Gehrels (2007b), Lower cretaceous strata in the Lhasa terrane, Tibet, with implications for understanding the early tectonic history of the Tibetan plateau, *J. Sediment. Res.*, *77*, 809–825, doi:10.2110/jsr.2007.078.

Leier, A. L., P. G. DeCelles, P. Kapp, G. E. Gehrels, and L. Ding (2007c), Detrital zircon geochronology of Phanerozoic sedimentary strata in the Lhasa terrane and implications for the tectonic evolution of southern Tibet, *Basin Res.*, *19*, 361–378, doi:10.1111/j.1365-2117.2007.00330.x.

Liu, Y., H. F. Liu, T. Theye, and H. J. Massonne (2010), Evidence for oceanic subduction at the NE Gondwana margin during Permo-Triassic times, *Terra Nova*, *21*(3), 195–202, doi:10.1111/j.1365-3121.2009.00874.x.

Ludwig, K. R. (2012), Isoplot/ex, v. 3.75, Berkeley geochronology center special Publlication 5.

Marcoux, J., J. Girardeau, E. Fourcade, J. P. Bassoullet, J. Philip, M. Jaffrezo, X. C. Xiao, and C. F. Chang (1987), Geology and biostratigraphy of the jurrassic and low cretaceous series to the north of the Lhasa block (Tibet, China), *Geodin. Acta*, *1*(4–5), 313–325, doi:10.1080/09853111.1987.11105148.

Miall, A. D. (1978), Facies types and vertical profile models in braided river deposits: A summary, in *Fluvial Sedimentology*, *Canadian Society of Petroleum Geologists Memoir*, vol. 5, edited by A. D. Miall, pp. 597–604.

Molnar, P. (2005), Mio-Pliocene growth of the Tibetan plateau and evolution of east Asian climate, *Palaeontol. Electron.*, *8*(1), 1–23.

Morel, M. L. A., O. Nebel, Y. J. Nebel-Jacobsen, J. S. Miller, and P. Z. Vroon (2008), Hafnium isotope characterization of the GJ-1 zircon reference material by solution and laser-ablation MC-ICPMS, *Chem. Geol.*, *255*(1–2), 231–235, doi:10.1016/j.chemgeo.2008.06.040.

Murphy, M. A., A. Yin, T. M. Harrison, S. B. Dürr, Z. Chen, F. J. Ryerson, W. S. F. Kidd, X. Wang, and X. Zhou (1997), Did the indo-Asian collision alone create the Tibetan plateau?, *Geology*, *25*(8), 719–722, doi:10.1130/0091-7613(1997)025<0719:DTIACA>2.3.CO;2.

Orme, D. A., B. Carrapa, and P. Kapp (2015), Sedimentology, provenance and geochronology of the upper cretaceous-lower Eocene western Xigaze forearc basin, southern Tibet, *Basin Res.*, *27*, 387–411, doi:10.1111/bre.12080.

Orme, D. A., and A. K. Laskowski (2016), Basin analysis of the Albian–Santonian Xigaze Forearc, Lazi region, south-Central Tibet, *J. Sediment. Res.*, *86*, 894–913, doi:10.2110/jsr.2016.59.

Pan, G. T., J. Ding, D. S. Yao, and L. Q. Wang (2004) *Guide Book of 1:1,500,000 Geologic map of the Qinghai-Xizang (Tibet) Plateau and Adjacent Areas*, 148 pp., Cartographic Publishing House, Chengdu, China.

Pullen, A., P. Kapp, G. E. Gehrels, P. G. DeCelles, E. H. Brown, J. M. Fabijanic, and L. Ding (2008), Gangdese retroarc thrust belt and foreland basin deposits in the Damxung area, southern Tibet, *J. Asian Earth Sci.*, *33*(5–6), 323–336, doi:10.1016/j.jseaes.2008.01.005.

Raymo, M. E., and W. F. Ruddiman (1992),Tectonic forcing of late Cenozoic climate, *Nature*, *359*, 117–122, doi:10.1038/359117a0.

Richter, F. M., D. B. Rowley, and D. J. DePaolo (1992), Sr isotope evolution of seawater: The role of tectonics, *Earth Planet. Sci. Lett.*, *109*, 11–23, doi:10.1016/0012-821X(92)90070-C.

Ridgway, K. D., and P. G. DeCelles (1993), Stream-dominated alluvial fan and lacustrine depositional systems in Cenozoic strike-slip basins, Denali fault system, Yukon territory, Canada, *Sedimentology*, *40*(4), 645–666, doi:10.1111/j.1365-3091.1993.tb01354.x.

Sciunnach, D., and E. Garzanti (2012), Subsidence history of the Tethys Himalaya, *Earth Sci. Rev.*, *111*(1–2), 179–198, doi:10.1016/j.earscirev.2011.11.007.

Söderlund, U., P. J. Patchett, J. D. Vervoort, and C. E. Isachsen (2004), The $^{176}$Lu decay constant determined by Lu–Hf and U–Pb isotope systematics of Precambrian mafic intrusions, *Earth Planet. Sci. Lett.*, *219*(3–4), 311–324, doi:10.1016/S0012-821X(04)00012-3.

Sun, G. Y. (2015), Sedimentary evolution of the cretaceous Coqen basin (southern Tibet) and implications for early topographic growth on the Lhasa terrane, PhD dissertation, 143 pp., Nanjing Univ., Nanjing, China.

Sun, G. Y., X. M. Hu, H. D. Sinclair, M. K. BouDagher-Fadel, and J. G. Wang (2015), Late cretaceous evolution of the Coqen Basin (Lhasa terrane) and implications for early topographic growth on the Tibetan plateau, *Geol. Soc. Am. Bull.*, *127*(7–8), 1001–1020, doi:10.1130/B31137.1.

Wang, C. S., X. H. Li, Z. F. Liu, Y. L. Li, L. Jansa, J. G. Dai, and Y. S. Wei (2012), Revision of the cretaceous–Paleogene stratigraphic framework, facies architecture and provenance of the Xigaze forearc basin along the Yarlung Zangbo suture zone, *Gondwana Res.*, *22*, 415–433, doi:10.1016/j.gr.2011.09.014.

Wang, J. G., X. M. Hu, E. Garzanti, and F. Y. Wu (2013), Upper Oligocene-lower Miocene Gangrinboche conglomerate in the Xigaze area, southern Tibet: Implications for Himalayan uplift and paleo-Yarlung-Zangbo initiation, *J. Geol.*, *121*(4), 425–444, doi:10.1086/670722.

Wang, J. G., X. M. Hu, E. Garzanti, W. An, and X. C. Liu (2017), The birth of the Xigaze forearc basin in southern Tibet, *Earth Planet. Sci. Lett.*, *465*, 38–47, doi:10.1016/j.epsl.2017.02.036.

Wen, D. R., D. Y. Liu, S. L. Chung, M. F. Chu, J. Q. Ji, Q. Zhang, B. Song, T. Y. Lee, M. W. Yeh, and C. H. Lo (2008), Zircon SHRIMP U–Pb ages of the Gangdese batholith and implications for Neotethyan subduction in southern Tibet, *Chem. Geol.*, *252*, 191–201, doi:10.1016/j.chemgeo.2008.03.003.

Woodhead, J. D., and J. M. Hergt (2005), A preliminary appraisal of seven natural zircon reference materials for in situ Hf isotope determination, *Geostand. Geoanal. Res.*, *29*, 183–195: doi:10.1111/j.1751-908X.2005.tb00891.x.

Wu, F. Y., Y. H. Yang, L. W. Xie, J. H. Yang, and P. Xu (2006), Hf isotopic compositions of the standard zircons and baddeleyites used in U–Pb geochronology, *Chem. Geol.*, *234*, 105–126, doi:10.1016/j.chemgeo.2016.03.025.

Xie, L. W., Y. B. Zhang, H. H. Zhang, J. F. Sun, and F. Y. Wu (2008), In situ simultaneous determination of trace elements, U–Pb and Lu–Hf isotopes in zircon and baddeleyite, *Chin. Sci. Bull.*, *53*, 1565–1573, doi:10.1007/s11434-008-0086-y.

Yang, J. S., Z. Q. Xu, Z. L. Li, X. Z. Xu, T. F. Li, Y. F. Ren, H. Q. Li, S. Y. Chen, and P. T. Robinson (2009), Discovery of an eclogite belt in the Lhasa block, Tibet: A new border for paleo-Tethys?, *J. Asian Earth Sci.*, *34*, 76–89, doi:10.1016/j.jseaes.2008.04.001.

Yin, A., and T. M. Harrison (2000), Geologic evolution of the Himalayan–Tibetan orogen, *Annu. Rev. Earth Planet. Sci. 28*, 211–280.

Yin, J. X., J. T. Xu, C. J. Liu, and H. Li (1988), The Tibetan plateau: Regional stratigraphic context and previous work, *Philos. Trans. R. Soc. London, Ser. Math. Phys. Sci.*, *327*, 5–52.

Zhang, K. J., B. D. Xia, G. M. Wang, Y. T. Li, and H. F. Ye (2004), Early cretaceous stratigraphy, depositional environments, sandstone provenance, and tectonic setting of central Tibet, western China, *Geol. Soc. Am. Bull.*, *116*, 1202–1222, doi:10.1130/B25388.1.

Zhang, K. J., Y. X. Zhang, X. C. Tang, and B. D. Xia (2012), Late Mesozoic tectonic evolution and growth of the Tibetan plateau prior to the indo-Asian collision, *Earth Sci. Rev.*, *114*(3–4), 236–249, doi:10.1016/j.earscirev.2012.06.001.

Zhang, Q. H., L. Ding, F. L. Cai, X. X. Xu, L. Y. Zhang, Q. Xu, and H. Willems (2011), Early cretaceous Gangdese retroarc foreland basin evolution in the Selin co basin, central Tibet: Evidence from sedimentology and detrital zircon geochronology, in *Growth and Collapse of the Tibetan Plateau*, *Geol. Soc. Lond. Spec. Publ.*, vol. 353, edited by R. Gloaguen and L. Ratschbacher, pp. 27–44.

Zhu, D. C., Z. D. Zhao, Y. L. Niu, X. X. Mo, S. L. Chung, Z. Q. Hou, L. Q. Wang, and F. Y. Wu (2011a), The Lhasa terrane: Record of a microcontinent and its histories of drift and growth, *Earth Planet. Sci. Lett.*, *301*(1–2), 241–255, doi:10.1016/j.epsl.2010.11.005.

Zhu, D. C., Z. D. Zhao, Y. L. Niu, Y. Dilek, and X. X. Mo (2011b), Lhasa terrane in southern Tibet came from Australia, *Geology*, *39*(8), 727–730, doi:10.1130/G31895.1.

Zhu, D. C., S. M. Li, P. A. Cawood, Q. Wang, Z. D. Zhao, S. A. Liu, and L. Q. Wang (2016), Assembly of the Lhasa and Qiangtang terranes in central Tibet by divergent double subduction, *Lithos*, *245*, 7–17, doi:10.1016/j.lithos.2015.06.023.